

Probing Spectral Line Gradients Beyond One Effective Radius in NGC 3610

Justin H. Howell

Lick Observatory, University of California, Santa Cruz, CA 95064, USA

jhhowell@ucolick.org

Jean P. Brodie

Lick Observatory, University of California, Santa Cruz, CA 95064, USA

brodie@ucolick.org

Jay Strader

Lick Observatory, University of California, Santa Cruz, CA 95064, USA

strader@ucolick.org

Duncan A. Forbes

Centre for Astrophysics & Supercomputing, Swinburne University, Hawthorn, VIC 3122, Australia

dforbes@astro.swin.edu.au

Robert Proctor

Centre for Astrophysics & Supercomputing, Swinburne University, Hawthorn, VIC 3122, Australia

rproctor@astro.swin.edu.au

ABSTRACT

The outer region (0.75–1.25 r_e in the B -band) of the merger-remnant elliptical NGC 3610 is studied using extremely high signal to noise Keck spectra, with a supplementary spectrum of the galaxy center. Stellar population parameters — age, $[Z/H]$, $[\alpha/Fe]$ — are measured in several apertures along the slit. Using the multi-index simultaneous fitting method of Proctor et al. (2004), no significant stellar population gradients are detected in the outer parts of the galaxy. The overall gradients relative to the galaxy center are consistent with those found in many other early-type galaxies, though the metallicity gradient is much steeper than would be expected if NGC 3610 formed in a major merger event. Standard analysis methods using the $H\beta$ index are found to produce spurious radially variable gradients.

Subject headings: galaxies: abundances — galaxies: individual (NGC 3610)

1. Introduction

Many studies of the star formation histories of elliptical galaxies are restricted to central apertures (e. g. Jorgensen 1997; Kuntschner & Davies 1998; Trager et al. 2000a; Terlevich & Forbes 2002). The necessary observations are relatively simple, and allow useful measurements of the basic physical parameters (velocity dispersion, age, metallicity, and α -enhancement) in the centers of galaxies. However, radial gradients in these quantities provide dramatically greater leverage when comparing to galaxy formation models. The observational challenges are correspondingly great, particularly for gradients extending beyond one effective radius (r_e). Several studies to date (e. g. Carollo et al. 1993; Davies et al. 1993; Kobayashi & Arimoto 1999; Mehlert et al. 2003) have surveyed gradients in different samples of galaxies. All are in agreement that most ellipticals become less metal-rich with radius by approximately -0.2 dex per decade in r/r_e . As this gradient is much shallower than that predicted by monolithic collapse galaxy formation models (Carlberg 1984) the standard interpretation is that merger events dilute the gradients of monolithically-forming precursor galaxies (White 1980). The simulations of a large number of elliptical galaxies under CDM initial conditions by Kobayashi (2004) confirm these conclusions using more sophisticated and up to date physical models. None of the galaxies with the steepest metallicity gradients, < -0.35 dex per decade in radius, had undergone a major merger, and the average gradient for merger remnant galaxies was shallower than the average gradient for galaxies which formed via monolithic collapse. The simulations also indicated that the extent to which the metallicity gradient will change in a merger event depends on both the mass ratio of the two merging galaxies and the gas fraction in the two galaxies.

This study uses extremely high signal-to-noise (S/N) spectra to study gradients in the stellar population parameters of NGC 3610 out to $1.25 r_e$. NGC 3610 is an interesting and nearby (distance modulus $m - M = 32.65$; Tonry et al. 2001) elliptical galaxy. Because of the extraordinary amount of fine structure (7.6 Schweizer & Seitzer 1992), the most in any galaxy outside of the Toomre sequence (Toomre & Toomre 1972), NGC 3610 has long been suspected of being an intermediate-age merger remnant. The anomalously blue $B - V$ color of the galaxy (Goudfrooij et al. 1994; Idiart, Michard & de Freitas Pacheco 2002) suggests recent star formation. The photometric study of Silva & Bothun (1998) confirmed the presence of intermediate-age stars. Although Silva & Bothun argued that the cold stellar disk lying along the major axis (Scorza & Bender 1990; Whitmore et al. 1997; Rix & White 1992) is difficult to reconcile with predictions of a major merger origin for NGC 3610, the simulations of Barnes (2002) have shown that such disks are a natural by-product of mergers of gas-rich systems.

Spectral line index measurements of the center of NGC 3610 (Howell & Guhathakurta 2004; Denicoló et al. 2004) indicate that it contains a young and metal-rich stellar population. Furthermore, young and old globular cluster populations have been found in this system (Whitmore et al. 1997; Strader et al. 2003; Strader, Brodie & Forbes 2004). The young globular cluster population is of comparable age to the galaxy center, but of slightly lower metallicity. Many of the old globular clusters are metal-rich, indicating that at least one progenitor galaxy must have had a significant

bulge population.

If NGC 3610 is a remnant of a recent major merger event, it should have a metallicity gradient even shallower than that found in other early-type galaxies. The simulations of Bekki & Shioya (1999) predict gradients of between -0.03 and -0.13 dex per decade in radius in galaxies formed from mergers of late-type (bulgeless) spiral galaxies. No simulations are yet available for metallicity gradients in mergers involving early-type spirals.

The paper is organized as follows. In § 2 we describe the data and reduction procedures, along with detailed data analysis. Stellar population parameters are derived in § 3, and § 4 discusses the conclusions of this work.

2. Data

2.1. Observation and Data Reduction

Data were obtained using LRIS-B (Oke et al. 1995) on the Keck telescope in 2003 January and 2004 April as by-products of an ongoing program to measure the ages and metallicities of the globular cluster systems of many nearby elliptical galaxies, including NGC 3610. The April data includes the center of NGC 3610 with the $162''$ long slit lying along the major axis. The January slit was oriented at an intermediate angle between NGC 3610's major and minor axes and was off-center by $10''$. Figure 1 shows the slit orientation relative to the galaxy for this observation. This slit position was chosen to intersect two globular cluster candidates. In both cases the galaxy was positioned in the center of one half of the CCD, such that the galaxy signal would be read out entirely by one of the two amplifiers. Five 1800 s exposures were taken resulting in a total exposure time of 2.5 hours for the off-axis (January) data; the on-axis (April) data consist of a single 5 minute exposure. Seeing was $\sim 0.8''$ for the off-axis data and $\sim 0.6''$ for the on-axis spectrum. Spectral resolution is approximately 70 km/s, with a wavelength range from 3000\AA – 5500\AA , a dispersion of $0.63\text{\AA}/\text{pixel}$, and a spatial scale of $0.135''/\text{pixel}$. Flat fields, flux standards, and Lick index standard stars were also observed throughout each observing run.

Data reduction followed standard procedures. First, the LRIS bias subtraction routine was executed. Flat-fielding was performed for wavelengths greater than $\sim 3700\text{\AA}$ only, as the flat-field lamp produces almost no light at bluer wavelengths. All data bluer than this flat-field cutoff were ignored in subsequent analysis. Next, the sections of the CCD read out by each amplifier were corrected to a common dispersion and intensity scale. Wavelength calibration was performed in two dimensions using the standard longslit packages IDENTIFY, REIDENTIFY, FITCOORDS, and TRANSFORM in IRAF¹. Similar procedures to identify arc lamp reference lines and calculate the

¹IRAF is distributed by the National Optical Astronomy Observatories, which are operated by the Association of Universities for Research in Astronomy, Inc., under cooperative agreement with the National Science Foundation.

dispersion solution between pixel space and wavelength space exist in any other astronomical data reduction package. Cosmic rays were masked on the TRANSFORMed images. After TRANSFORM the galaxy spectrum was almost perfectly aligned with the CCD. The on-axis data was extracted, traced, and sky subtracted using the APALL task. The broad spatial brightness profile of the off-axis data precluded sufficiently accurate centroid measurement for an aperture to be traced by APALL, so extraction was performed by combining rows of the CCD directly. A sky aperture was defined consisting of a $13.5''$ region at the far edge of the CCD from the galaxy spectrum. At over $7r_e$ the contribution of galaxy light to this sky spectrum is completely negligible. This sky spectrum was subtracted from each row of each of the galaxy apertures before the galaxy spectra were extracted.

Six galaxy apertures were defined with S/N per pixel of 120 in each. At such high S/N , Poisson errors have become negligible compared to the various sources of calibration error, not to mention the internal uncertainties within the Lick/IDS system. The minimum aperture size was several times as large as the seeing. The outermost apertures were restricted to go no further than the point at which the galaxy intensity fell below twice the sky intensity. These apertures have been labeled in pairs. The innermost pair is ‘A’, the middle pair is ‘B’, and the outer pair is ‘C’. Within each pair, the aperture closer to the minor axis of the galaxy is ‘1’ while the aperture closest to the major axis is ‘2’. For the on-axis spectrum, a central aperture was defined extending to $r_e/8$, and two flanking apertures between $r_e/8$ and the above sky cutoff ($\sim 1 r_e$ in this case) were also extracted using the trace from the $r_e/8$ aperture. All of these extractions were averages set to exclude the cosmic rays and bad pixels which were masked earlier. After extraction, the one-dimensional spectra were flux calibrated using standard techniques.

2.2. Velocity Dispersion Correction and Lick Index Measurements

When measuring spectral indices in galaxies, it is necessary to correct for the effect of the galaxy’s velocity dispersion broadening the absorption lines. This is critical both for meaningful comparisons to stellar population models and for comparisons between different apertures, which in general have slightly different velocity dispersions. This correction was done by matching model spectra from Schiavon (2004) to the galaxy spectra. The major difference between these model spectra and previous work is the use of the Jones spectral library (Jones 1999) for deriving the fitting functions for spectra of particular ages and metallicities. Unlike other models based on this library, the atmospheric parameters for the library stars are entirely new. In addition, these models provide synthetic SSP spectra, which are used in the velocity dispersion correction. The velocity dispersion (σ) for each aperture was measured using the Pixfit code (van der Marel 1994), which broadens a model spectrum by a user-defined range of σ values and determines the best fit by chi-squared minimization between the broadened model spectra and the data. The resulting σ measurements were used to smooth the best fitting models in order to derive a σ -correction. The galaxy and model spectra (both for $\sigma = 0$ and $\sigma = \sigma_{3610}$ varying from 135 to 180 km/s depending on aperture) were degraded to match the Lick/IDS resolution (Worthey & Ottaviani 1997). The

smoothing for the blue part of the spectrum was performed piecewise in 100\AA increments, as the Lick/IDS resolution varies strongly with wavelength in that region.

Equivalent widths of the Lick/IDS indices defined in Trager et al. (1998) and Worthey & Ottaviani (1997) were measured using a modified version of the `bwid` program provided by R. M. Rich (Rich 1998). A sample spectrum (not degraded to IDS resolution) is shown in Figure 2 with the Lick/IDS indices and the location of $[\text{OIII}]\lambda 5007$ marked. For each line index, the multiplicative correction applied to the galaxy measurements was the ratio of the $\sigma = 0$ model index to the model index smoothed to the galaxy’s velocity dispersion. Lick index standard stars (six from the off-axis observing run, three from the on-axis observing run) were reduced identically to the galaxy spectra, and offsets were determined to calibrate these data to the Lick system. The RMS scatter of the standard star index measurements relative to the Lick system is $0.03\text{--}0.08\text{\AA}$ for most indices, with Fe5015 and $\text{H}\delta_{\text{F}}$ being more uncertain. The $\text{H}\delta_{\text{F}}$ calibration is especially uncertain due to a poor match of standard stars to the galaxy in that index.

NGC 3610 shows very little emission at $[\text{OIII}]\lambda 5007$. However, in a few apertures from the off-axis spectra this emission, while very small, is non-zero and may affect several absorption lines. The $[\text{OIII}]$ line was used to correct $\text{H}\beta$ via Equation 2 of Trager et al. (2000a). The $\text{H}\delta_{\text{F}}$, $\text{H}\gamma_{\text{F}}$, and Fe5015 indices were corrected as described in Kuntschner et al. (2002). This measurement was done independently for each of the five exposures; the mean value and the error in the mean for each aperture were used in all emission correction calculations.

The index measurements for each aperture are presented in Table 1 along with the total observational error calculated below. Also listed are the measurements from the combined spectrum of all six off-axis apertures (Fig. 2). The luminosity-weighted median radius of each aperture is presented in Table 2 in units of the effective radius at that angle from the center of the galaxy. The mean B -band effective radius of NGC 3610 was taken from Faber et al. (1989) while the axis ratio was measured from a direct image taken along with the off-axis spectra.

2.3. Errors

The total errors for each index in each aperture were measured as follows. The five independently reduced observations provide a direct measure of the random Poisson error for the off-axis apertures. Sky subtraction error was measured by determining the index offsets when the sky level was over- or undersubtracted by 1.4%, the estimated Poisson uncertainty in the sky intensity. Wavelength calibration error contributes significantly in this instrument and lamp setup. The best wavelength solution had an rms error of 0.40\AA . This was translated into index errors by shifting the spectra by that amount and noting the extent of the offset. Radial velocity uncertainty was slightly less than wavelength calibration error in magnitude, and was treated identically. Velocity dispersion corrections are known to be very index-dependent (Trager et al. 1998). The fitting functions from that work were used to translate a conservative estimate $\sigma_{\sigma} \approx 10 \text{ km/s}$ into index

errors. Finally, the error in measuring [OIII] λ 5007 emission was estimated as described above and propagated into $\sigma_{H\beta}$, $\sigma_{H\gamma}$, $\sigma_{H\delta}$, and σ_{Fe5015} .

Errors in calibration to the Lick/IDS system were determined from the residuals of the standard star offset fits. As is typical of Lick index studies, these calibration errors are significant and often dominate the error budget. However, they are less important for our purposes, since we are primarily interested in differential effects.

Although not a concern for the analysis technique of § 3.1, uncertainties within the Lick/IDS data set are necessary for the fitting procedure of § 3.2. Errors for each index were taken from Worthey, Faber, Gonzalez, & Burstein (1994) and Worthey & Ottaviani (1997). Since each standard star was given equal weight in the calibration to the Lick/IDS system, the IDS internal error was calculated as the average of the errors in the individual stars, weighted by the number of IDS observations. As per Worthey, Faber, Gonzalez, & Burstein (1994), errors for IDS standard stars, of which two were observed in January and one in April, were reduced by a further factor of 1.2.

Errors from all sources are listed individually in Table 2. From these, a total error was calculated for each index in each aperture. For this purpose the Poisson noise error was ignored as it is already incorporated within many of the other error sources. The uncertainty within the Lick/IDS system, σ_{IDS} , was also excluded from the formal error quoted in Table 1 as it represents a purely systematic error. The remaining sources of error were added in quadrature to determine the total observational error. Note that although several of these error sources (e.g. Lick/IDS calibration, sky subtraction, wavelength calibration) involve systematic corrections, the errors are random. For example, sky subtraction involves subtracting the same sky spectrum from each aperture on an image. But it is entirely reasonable to suppose that the actual sky intensity will vary slightly from pixel to pixel in the spatial direction within each aperture. Thus the sky at each row of the CCD will be over- or undersubtracted by a small and random amount, resulting in random sky subtraction error.

3. Results

Before proceeding to measure stellar population parameters, gradients in individual indices can be measured. The Mg_2 index is most commonly used for this purpose (e. g. Davies et al. 1993; Kobayashi & Arimoto 1999). The Mg_2 gradient in NGC 3610 is presented in Fig. 3; the gradient of $\Delta Mg_2 / \Delta \log(r/r_e) = -0.056 \pm 0.004$ is in excellent agreement with previous work on large samples of elliptical galaxies. It is also worth noting that within the off-axis apertures the Mg_2 measurements are systematically larger in the apertures nearest the major axis (A2–C2).

3.1. Single Stellar Population Models

The age and mean metallicity of NGC 3610 were estimated from single stellar population (SSP) model grids of Thomas, Maraston & Bender (2003) in the $H\beta$ – $[MgFe]'$ plane. Balmer indices such as $H\beta$ are primarily age-sensitive, while the composite index $[MgFe]'$ was defined by Thomas et al. (2003) as a metallicity-sensitive index which is not affected by variations in $[\alpha/Fe]$. Thus by plotting data and model grids in Balmer index vs. $[MgFe]'$ space (any metal index can be used if $[\alpha/Fe]$ is not expected to be variable) one can interpolate the SSP age and metallicity for each observation. Note that most galaxies did not form in a single starburst, so the SSP parameters reflect luminosity-weighted mean values not the true age, metallicity, and $[\alpha/Fe]$ of the galaxy. Fig. 4 shows a mean age of approximately 1.9 Gyr, with $[Z/H] \sim +0.2$ averaged over the off-axis data points. Moreover, there is a clear and significant gradient within the off-axis apertures in the sense that the stars in the outermost apertures are younger and more metal-rich than those in the innermost apertures. This trend is not statistically significant in similar grids using $H\gamma$ and $H\delta$ (Figs. 5 & 6), however. Note that although the gradients in individual metal lines and the higher order Balmer lines (see Table 1) are only marginally statistically significant at best, the $H\beta$ gradient is highly significant. The average $H\beta$ measurement in apertures C1 and C2 is higher by more than four standard deviations than the average $H\beta$ measurement in apertures A1 and A2.

Variations in $[\alpha/Fe]$ with radius were measured from the same models. The 2.0 Gyr models were linearly interpolated in the $Mg\ b < Fe >$ plane (Fig. 7). The offsets perpendicular to the iso-enhancement lines between the 2.0 Gyr models and the 1.0 and 3.0 Gyr models were used to interpolate an age correction to the final $[\alpha/Fe]$ measurements. Five apertures have nearly identical $[\alpha/Fe] \sim 0.25$, while aperture C2 is more α -enhanced.

The on-axis data set extends the radial range of stellar population measurements inwards to the center of NGC 3610. The central $r_e/8$ aperture (labelled Center in Table 1; small square in Figs. 4–7) is in good agreement with previous work (Howell & Guhathakurta 2004; Denicoló et al. 2004). Metallicity is much higher in the center of the galaxy than in the 0.75 – $1.25\ r_e$ region, while age and $[\alpha/Fe]$ are found to be consistent with the average values in the outer apertures. The two flanking apertures (N and P in Table 1; averaged together and plotted as the large square in Figs. 4–7) provide an intermediate measurement between the center and the off-axis apertures. Metallicity is between that of the center and the off-axis apertures, but $[\alpha/Fe]$ is slightly higher than in either the center or the off-axis apertures. Age is unclear — $H\beta$ and $H\gamma$ suggest a slightly younger age than the center and most or all of the off-axis apertures, while $H\delta$ suggests that all three regions are coeval. On average the three regions of NGC 3610 ($r_e/8$, intermediate, and off-axis apertures) show a metallicity gradient with no significant trends in age or $[\alpha/Fe]$. However the detailed radial stellar population profile, taking into account the individual off-axis apertures apparently becoming younger and more metal rich with radius (Fig. 4), is implausibly variable. Metallicity decreases outwards to the off-axis apertures, then increases; age decreases slightly, then increases at the innermost off-axis apertures and sharply decreases.

It is important to rule out uncorrected instrumental bias or systematic error as the cause of these unusual gradients. This possibility has been carefully examined. Since many age and metallicity indices, including $H\beta$, Mgb , $Fe5270$, and $Fe5335$, increase with radius one might imagine that the gradients in age and metallicity arise from oversubtracting sky light. This was tested by rereducing the data with 10% less sky subtracted, an amount far in excess of the Poisson error in the sky intensity. Even in this extreme case, the sense of the gradients measured in this study was preserved, though naturally the quantitative details were different. Additional experiments showed that the gradients are minimized if approximately 20% less sky is subtracted. Furthermore, if sky oversubtraction was a problem one would expect that *all* indices would follow the trend of increasing monotonically with radius. Table 1 shows that this is not the case. An incorrect sky measurement cannot be the source of the observed gradients.

Scattered light is another potential source of instrumental contamination of our results. Tests were performed by Javier Cenarro in which stellar spectra were convolved with the spatial brightness profile of the off-axis NGC 3610 data and then extracted and measured identically to the galaxy apertures (Cenarro, private communication). Slight gradients due to scattered light were detected, but of very small degree, in all cases less than the index errors. These scattered light gradients also generally had the opposite sign of the observed galaxy gradients. We conclude that scattered light contamination is not a problem.

Having ruled out the plausible sources of systematic error, two possibilities remain. Either NGC 3610 really does have an implausible radially varying stellar population gradient as suggested by Fig. 4, or the standard stellar population measurement technique using the $H\beta$, Mgb , $Fe5270$, and $Fe5335$ indices is flawed. Stellar population measurements using $H\gamma$ and $H\delta$ instead of $H\beta$ do not resolve this question. As shown in Figs. 5 and 6 respectively, the observations hint at the age gradient within the off-axis apertures seen in Fig. 4 but not at a statistically significant level. An independent stellar population fitting method allows these possibilities to be addressed.

3.2. Multiple Index Fitting

The technique of Proctor et al. (2004) provides a robust method of measuring age, metallicity, and α -enhancement in galaxy spectra. Briefly, this involves the creation of a three-dimensional grid of $\log t$, $[Fe/H]$, and $[\alpha/Fe]$, with model values for each Lick index at each point in the grid calculated from the solar abundance ratio SSPs of Thomas et al. (2003) and modified according to Tripicco & Bell (1995) to reflect variations in $[\alpha/Fe]$. These $[\alpha/Fe]$ calculations were performed using the Fe- method from Proctor & Sansom (2002). A χ^2 fit is then performed to find the best fit model parameters to the set of indices observed in a particular galaxy. The use of every observed index in the fit has the advantage of allowing deviant indices, whether from sky subtraction residuals, emission contamination, or other problems, to be omitted from the fit while still producing reliable measurements of the galaxy parameters. It has been shown that ages can be measured even if all Balmer indices are excluded (Proctor & Sansom 2002), for example. For this calculation the

systematic uncertainty within the Lick/IDS system was added in quadrature to the observational errors.

No significant gradient is measured in any parameter between 0.75–1.25 r_e (Fig. 8). Slight offsets (1–2 standard deviations) in age and metallicity are found between the apertures closest to the galaxy major axis (A2–C2) and their counterparts closer to the minor axis, with the major axis apertures being younger and more metal-rich. It is possible the disk population may preferentially add young, metal-rich stars to these apertures. However, the observed disk component of NGC 3610 is very small (Scorza & Bender 1990; Whitmore et al. 1997; Rix & White 1992), extending to only a few arcseconds. It is unclear how such a disk could produce much effect at distances beyond 1 r_e . A gradient in metallicity is found between the center of the galaxy and the off-axis apertures, -0.30 ± 0.05 dex in $[Z/H]$ per decade in radius. The gradients in age and $[\alpha/Fe]$ have a statistical significance of $< 2\sigma$ over the radial range, hinting that the galaxy center might be slightly younger and more α -enhanced relative to the outer parts. Age and metallicity were also found to be quantitatively different than those measured in § 3.1 in the sense that the multi-index fit measures older ages and lower $[Z/H]$. $H\beta$ was found to be approximately 0.15 Å too large compared to the best fit value in all apertures. However, excluding it or any other index does not alter these conclusions but only reduces the χ^2 value of the fits.

As a consistency check, this multi-index fitting procedure was run using just the $H\beta$, Mgb , $Fe5270$, and $Fe5335$ indices. The results were very similar to those presented in § 3.1 based on two dimensional grids of combinations of those four indices (Fig. 9). The multi-index fits were in good quantitative agreement in both age and metallicity, systematically offset by ~ 0.03 dex in the former and ~ -0.1 dex in the latter relative to the two dimensional fits. The metallicity gradient using just these four indices remained the same using either fitting technique. This shows that the different stellar population measurements from the full multi-index fit are not artifacts of the fitting software, but reflect real physical information gained by using the additional ten indices in the fit.

4. Discussion and Conclusions

An extremely high S/N long slit spectrum of the outer parts of NGC 3610 has been obtained using the Keck telescope. Lick indices have been measured in six apertures along the slit, spanning the major and minor axes of the galaxy. Indices were also measured in three supplementary apertures on a central spectrum lying along the galaxy major axis. Stellar population parameters were measured using both the traditional methods involving two dimensional grids of a few Lick indices and using a multi-index fitting procedure that determines age, $[Z/H]$, and $[\alpha/Fe]$ simultaneously using every available index. Using $H\beta$ as the age-sensitive index, the traditional method indicated a variable and physically implausible radial gradient in age and metallicity, though only the metallicity gradient was statistically significant if higher order Balmer lines were used instead of $H\beta$. The multi-index fitting technique produced consistent results using the same limited set of

indices, but yielded a different set of gradients once all available indices were utilized. The outer apertures are consistent with a flat population gradient, and when combined with the interior data points the overall gradients from the galaxy center out beyond $1 r_e$ are qualitatively consistent with the conclusions of previous studies (Davies et al. 1993; Kobayashi & Arimoto 1999; Saglia et al. 2000; Mehlert et al. 2003) based on samples of other elliptical galaxies: age and $[\alpha/\text{Fe}]$ do not vary significantly with radius, while $[\text{Z}/\text{H}]$ decreases with radius. The overall gradient in $[\text{Z}/\text{H}]$ is -0.30 dex per decade in r/r_e , in agreement with the sample of Kobayashi & Arimoto (1999) but slightly larger than the typical values quoted in the other studies. For example, high redshift formation models by Pipino & Matteucci (2004) predict shallow gradients, ~ -0.12 in cases where the $[\alpha/\text{Fe}]$ gradient is small, as is the case in NGC 3610.

Since mergers are expected to flatten a galaxy’s metallicity gradient (White 1980), it is intriguing that NGC 3610 has a relatively steep gradient despite a wealth of merger remnant signatures (young age, young globular clusters, much fine structure, stellar disk). Models of metallicity gradients in remnants of mergers between pure disk progenitor galaxies predict very shallow gradients, -0.03 to -0.13 dex per decade in radius, depending on galaxy mass (10^{10} – $10^{12}M_\odot$; Bekki & Shioya 1999). The old metal-rich globular cluster population of NGC 3610 indicates that at least one progenitor galaxy had a significant bulge component (Strader, Brodie & Forbes 2004), assuming NGC 3610 did indeed form via a major merger event. However, the presence of a bulge might act to inhibit gas flow to the center of the merger, so it is not clear that interaction models with bulges would produce steeper gradients. The CDM chemodynamical simulations of Kobayashi (2004) indicate that the gradient observed in NGC 3610 is still consistent with a major merger history, though steeper than typical for major merger remnants.

A very important ancillary conclusion is that the use of only a few Lick indices at a time can produce misleading results, particularly if the age-sensitive index chosen is $\text{H}\beta$. Several factors can lead to such biases. The Balmer lines, traditionally the primary age indicators among the set of Lick indices, can be contaminated by emission from star forming regions. The $\text{H}\beta$ index, which in many studies is the only Balmer line available, is most strongly affected by such emission. As described above, emission corrections can be made but such corrections are notoriously unreliable. As shown by Fig. 4, this is not a major problem in NGC 3610 as only a few apertures showed any $[\text{OIII}]\lambda 5007$ emission, and such emission was always small. A more serious problem with the $\text{H}\beta$ index was pointed out by Strader & Brodie (2004). Their principal components analysis of Galactic globular cluster indices suggests a nonlinear component to the relation between $\text{H}\beta$ and metallicity, driven by weak Fe I lines within the $\text{H}\beta$ index passbands. This nonlinear relation is expected to produce spurious spreads in ages derived using $\text{H}\beta$ compared to ages derived from higher order Balmer lines — precisely the effect seen in the off-axis apertures (Figs. 4–6). Recall that of the off-axis indices used in §3.1, $\text{H}\beta$ was the most variable, the only index with radial variations that were clearly statistically significant. A study of Galactic globular clusters (Proctor, Forbes & Beasley 2004) has also shown a spurious spread in derived ages resulting from the use of $\text{H}\beta$.

Depending on the set of Lick index standard stars observed, differences in calibration uncer-

tainty can also yield unreliable results if poorly calibrated indices are used. Two indices, $H\delta_F$ and Fe5015, suffered from this effect in the case of NGC 3610. As long as the errors are accurately determined, the multi-index fitting procedure can use even quite uncertain indices. Attempting to measure anything using two dimensional grids of such indices will at best lead to results of low statistical significance. In principle several other issues such as night sky line residuals can also contaminate individual index measurements, and thus any stellar population measurements made using primarily that index. Such indices would be easily flagged as outliers in a multi-index fitting technique which forces a stellar population fit to be consistent with every index measurement.

5. Acknowledgments

We thank Ricardo Schiavon, Raja Guhathakurta, Glenda Denicoló, Bill Mathews, and Mike Beasley for helpful discussions. We are grateful to Javier Cenarro for running scattered light tests. DF and RP thank the ARC for their financial support. We acknowledge support by the National Science Foundation through Grant AST-0206139. We thank the anonymous referee for helpful comments.

REFERENCES

- Barnes, J. E. 2002, *MNRAS*, 333, 481
- Bekki, K. & Shioya, Y. 1999, *ApJ*, 513, 108
- Bruzual, G. & Charlot, S. 2003, *MNRAS*, 344, 1000
- Carlberg, R. G. 1984, *ApJ*, 286, 403
- Carollo, C. M., Danziger, I. J. & Buson, L. 1993, *MNRAS*, 265, 553
- Davies, R. L., Sadler, E. M. & Peletier, R. F. 1993, *MNRAS*, 262, 650
- Denicoló, G., Terlevich, R., Terlevich, E., Forbes, D. A., Terlevich, A. & Carrasco, L. 2004, *MNRAS*, in preparation
- Faber, S. M., Wegner, G., Burstein, D., Davies, R. L., Dressler, A., Lynden-Bell, D. & Terlevich, R. J. 1989, *ApJS*, 69, 763
- Goudfrooij, P., Hansen, L., Jorgensen, H. E., Norgaard-Nielsen, H. U., de Jong, T. & van den Hoek, L. B. 1994, *A&AS*, 104, 179
- Howell, J. H. & Guhathakurta, P. 2004, in preparation
- Idiart, T. P., Michard, R. & de Freitas Pacheco, J. A. 2002, *A&A*, 383, 30

- Jones, L.A. 1999, PhD Thesis, University of North Carolina
- Jorgensen, I. 1997, MNRAS, 288, 161
- Kobayashi, C. & Arimoto, N. 1999, ApJ, 527, 573
- Kobayashi, C. 2004, MNRAS, 347, 740
- Kuntschner, H. & Davies, R. L. 1998, MNRAS, 295, L29
- Kuntschner, H., Smith, R. J., Colless, M., Davies, R. L., Kaldare, R. & Vazdekis, A. 2002, MNRAS, 337, 172
- Mehlert, D., Thomas, D., Saglia, R. P., Bender, R. & Wegner, G. 2003, A&A, 407, 423
- Oke, J. B., et al. 1995, PASP, 107, 375
- Pipino, A. & Matteucci, F. 2004, MNRAS, 347, 968
- Proctor, R. N., Forbes, D. A., Hau, G. K. T., Beasley, M. A., De Silva, G. M., Contreras, R., & Terlevich, A. I. 2004, MNRAS, 349, 1381
- Proctor, R. N. & Sansom, A. E. 2002, MNRAS, 333, 517
- Proctor, R. N., Forbes, D. A., & Beasley, M. A. 2004, MNRAS, submitted
- Rich, R. M. 1998, ASP Conf. Ser. 147, Abundance Profiles: Diagnostic Tools for Galaxy History, ed. D. Friedli, M. Edmunds, C. Robert & L. Drissen (San Francisco: ASP), p. 36
- Rix, H. & White, S. D. M. 1992, MNRAS, 254, 389
- Saglia, R. P., Maraston, C., Greggio, L., Bender, R. & Ziegler, B. 2000, A&A, 360, 911
- Schiavon, R. 2004, in preparation
- Schweizer, F. & Seitzer, P. 1992, AJ, 104, 1039
- Scorza, C. & Bender, R. 1990, A&A, 235, 49
- Silva, D. R. & Bothun, G. D. 1998, AJ, 116, 2793
- Strader, J., Brodie, J., Schweizer, F., Larsen, S. & Seitzer, P. 2003, AJ, 125, 626
- Strader, J., Brodie, J. & Forbes, D. A. 2004, AJ, 127, 295
- Strader, J. & Brodie, J. 2004, AJ, accepted
- Terlevich, A. I. & Forbes, D. A. 2002, MNRAS, 330, 547
- Thomas, D., Maraston, C. & Bender, R. 2003, MNRAS, 339, 897

Tonry, J. L., Dressler, A., Blakeslee, J. P., Ajhar, E. A., Fletcher, A. B., Luppino, G. A., Metzger, M. R. & Moore, C. B. 2001, ApJ, 546, 681

Toomre, A. & Toomre, J. 1972, ApJ, 178, 623

Trager, S. C., Worthey, G., Faber, S. M. & Gonzalez, J. J. 1998, ApJS, 116, 1

Trager, S. C., Faber, S. M., Worthey, G. & Gonzalez, J. J. 2000a, AJ, 119, 1645

Tripicco, M. J. & Bell, R. A. 1995, AJ, 110, 3035

van der Marel 1994, MNRAS, 270, 271

Vazdekis, A. 1999, ApJ, 513, 224

White, S. D. M. 1980, MNRAS, 191, 1P

Whitmore, B. C., Miller, B. W., Schweizer, F. & Fall, S. M. 1997, AJ, 114, 1797

Worthey, G., Faber, S. M., Gonzalez, J. J., & Burstein, D. 1994, ApJS, 94, 687

Worthey, G. & Ottaviani, D. L. 1997, ApJS, 111, 377

Table 1. Index table

Aperture Errors	Ca4227	G4300	Fe4383	Ca4455	Fe4531	C4668	H β	Fe5015	Mg ₂	Mgb	Fe5270	Fe5335	Fe5406	H δ_F	H γ_F
A1	0.81	4.68	4.46	1.14	3.12	4.52	2.38	4.94	0.205	3.27	2.55	2.00	1.31	1.62	-0.04
σ	0.05	0.10	0.12	0.10	0.05	0.08	0.04	0.14	0.002	0.07	0.05	0.09	0.06	0.21	0.03
A2	0.80	4.64	4.41	1.17	3.11	4.70	2.40	4.77	0.209	3.36	2.64	2.09	1.36	1.65	-0.01
σ	0.05	0.10	0.12	0.10	0.05	0.08	0.04	0.14	0.002	0.07	0.05	0.09	0.06	0.21	0.03
B1	0.87	4.68	4.39	1.15	3.02	4.57	2.35	4.84	0.203	3.32	2.60	2.00	1.37	1.60	-0.05
σ	0.05	0.10	0.12	0.10	0.05	0.08	0.04	0.14	0.002	0.07	0.05	0.09	0.06	0.21	0.03
B2	0.75	4.75	4.42	1.20	3.06	4.79	2.47	4.72	0.209	3.36	2.64	2.07	1.35	1.75	0.00
σ	0.05	0.10	0.12	0.11	0.05	0.08	0.05	0.14	0.002	0.07	0.05	0.09	0.06	0.21	0.03
C1	0.83	4.67	4.55	1.22	3.13	4.33	2.55	4.78	0.196	3.36	2.74	2.04	1.37	1.80	0.00
σ	0.05	0.11	0.13	0.11	0.06	0.08	0.05	0.14	0.002	0.07	0.05	0.09	0.07	0.22	0.04
C2	0.80	4.73	4.74	1.31	3.21	4.81	2.70	4.79	0.210	3.52	2.74	2.01	1.41	1.71	0.03
σ	0.05	0.12	0.14	0.11	0.06	0.09	0.05	0.14	0.002	0.08	0.05	0.09	0.06	0.21	0.04
All	0.76	4.81	4.25	1.44	2.94	4.60	2.54	4.91	0.206	3.36	2.63	2.13	1.37	1.58	-0.06
σ	0.05	0.09	0.11	0.10	0.05	0.08	0.04	0.14	0.002	0.07	0.05	0.09	0.06	0.21	0.03
Center	0.86	5.57	5.14	1.78	3.92	7.46	2.38	6.26	0.270	4.05	2.86	2.60	1.73	1.01	-0.52
σ	0.09	0.23	0.09	0.11	0.19	0.21	0.03	0.27	0.004	0.14	0.18	0.07	0.04	0.19	0.05
N	0.81	5.07	4.45	1.51	3.77	5.60	2.57	5.60	0.241	3.96	2.65	2.15	1.49	1.26	-0.01
σ	0.09	0.24	0.13	0.12	0.19	0.22	0.04	0.27	0.004	0.14	0.18	0.07	0.06	0.20	0.06
P	0.82	5.18	4.53	1.58	3.75	5.84	2.51	5.86	0.236	3.80	2.64	2.14	1.46	1.35	0.06
σ	0.09	0.24	0.13	0.12	0.19	0.22	0.04	0.27	0.004	0.14	0.18	0.07	0.06	0.20	0.06

Table 2. Error table

Error	Ca4227	G4300	Fe4383	Ca4455	Fe4531	C4668	H β	Fe5015	Mg ₂	Mgb	Fe5270	Fe5335	Fe5406	H δ_F	H γ_F
Aperture A1: $0.77 r_e(-33^\circ)$															
$\sigma_{\text{pois},3}$	0.01	0.02	0.06	0.03	0.03	0.03	0.03	0.05	0.001	0.02	0.04	0.03	0.01	0.05	0.01
$\sigma_{\text{sky},3}$	0.004	0.03	0.03	0.003	0.01	0.02	0.01	0.008	0.0	0.01	0.01	0.007	0.003	0.008	0.008
Aperture A2: $0.75 r_e(-16^\circ)$															
$\sigma_{\text{pois},4}$	0.02	0.04	0.05	0.03	0.03	0.04	0.02	0.06	0.002	0.01	0.02	0.02	0.04	0.06	0.02
$\sigma_{\text{sky},4}$	0.006	0.03	0.03	0.004	0.01	0.02	0.01	0.008	0.0	0.01	0.01	0.007	0.003	0.008	0.008
Aperture B1: $0.91 r_e(-54^\circ)$															
$\sigma_{\text{pois},2}$	0.03	0.03	0.06	0.04	0.05	0.03	0.03	0.08	0.002	0.03	0.05	0.03	0.07	0.02	0.04
$\sigma_{\text{sky},2}$	0.007	0.03	0.04	0.004	0.01	0.02	0.01	0.01	0.0	0.02	0.01	0.007	0.004	0.01	0.01
Aperture B2: $0.86 r_e(0^\circ)$															
$\sigma_{\text{pois},5}$	0.02	0.04	0.1	0.02	0.07	0.04	0.04	0.04	0.002	0.04	0.05	0.02	0.03	0.03	0.03
$\sigma_{\text{sky},5}$	0.007	0.04	0.04	0.006	0.02	0.02	0.02	0.01	0.0	0.02	0.02	0.01	0.004	0.01	0.01
$\sigma_{\text{emission},5}$	–	–	–	–	–	–	0.02	0.02	–	–	–	–	–	0.006	0.01
Aperture C1: $1.26 r_e(-81^\circ)$															
$\sigma_{\text{pois},1}$	0.05	0.01	0.10	0.02	0.04	0.08	0.02	0.10	0.003	0.05	0.06	0.03	0.03	0.06	0.05
$\sigma_{\text{sky},1}$	0.01	0.06	0.07	0.007	0.03	0.02	0.03	0.03	0.0	0.01	0.008	0.02	0.02	0.04	0.03
$\sigma_{\text{emission},1}$	–	–	–	–	–	–	0.01	0.01	–	–	–	–	–	0.003	0.005
Aperture C2: $1.23 r_e(14^\circ)$															
$\sigma_{\text{pois},6}$	0.04	0.03	0.05	0.03	0.06	0.07	0.07	0.10	0.003	0.03	0.06	0.05	0.07	0.04	0.02
$\sigma_{\text{sky},6}$	0.01	0.07	0.08	0.01	0.03	0.04	0.03	0.02	0.0	0.04	0.03	0.02	0.008	0.02	0.02
$\sigma_{\text{emission},6}$	–	–	–	–	–	–	0.01	0.01	–	–	–	–	–	0.003	0.005
Errors independent of aperture															
σ_λ	0.02	0.05	0.06	0.08	0.02	0.02	0.02	0.06	0.0	0.0	0.008	0.006	0.0	0.02	0.01
σ_{v_r}	0.02	0.04	0.05	0.06	0.02	0.02	0.01	0.04	0.0	0.0	0.006	0.005	0.0	0.02	0.01
σ_σ	0.009	0.0	0.0	0.01	0.0	0.0	0.0	0.0	0.0	0.02	0.0	0.03	0.02	0.0	0.0
σ_{cal}	0.04	0.07	0.08	0.03	0.04	0.07	0.03	0.12	0.002	0.07	0.04	0.08	0.06	0.21	0.03
σ_{IDS}	0.08	0.12	0.17	0.08	0.13	0.20	0.07	0.14	0.003	0.07	0.09	0.08	0.06	0.13	0.10

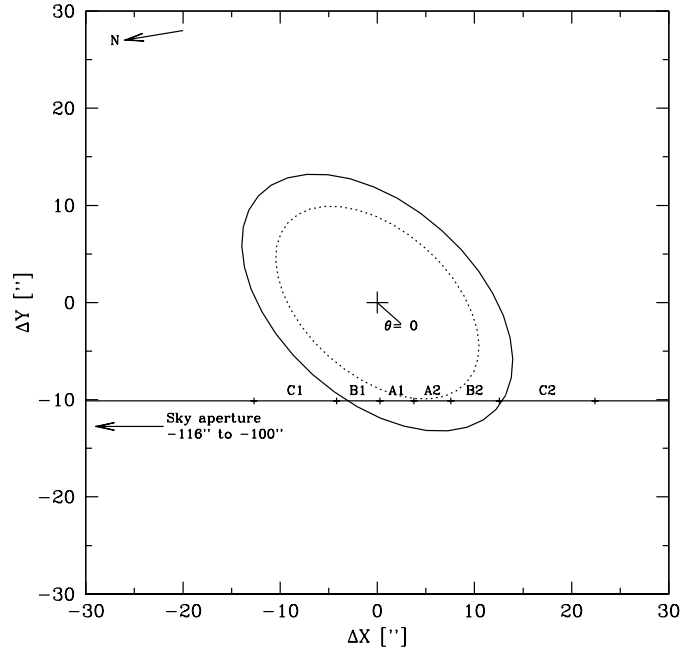


Fig. 1.— A diagram showing the orientation of the off-axis slit from the January data with respect to NGC 3610. The solid ellipse is a contour of $1 r_e$, and the dotted ellipse is a contour of $0.75 r_e$. The horizontal line shows the position of the slit, with tickmarks at the bounds of each of the six apertures. Apertures A1 and A2 are the closest to the galaxy center, on the minor and major axis sides respectively; the B and C apertures follow the same numbering pattern at progressively larger galactocentric radii. The angle θ with respect to the galaxy center is defined relative to the southeastern semimajor axis.

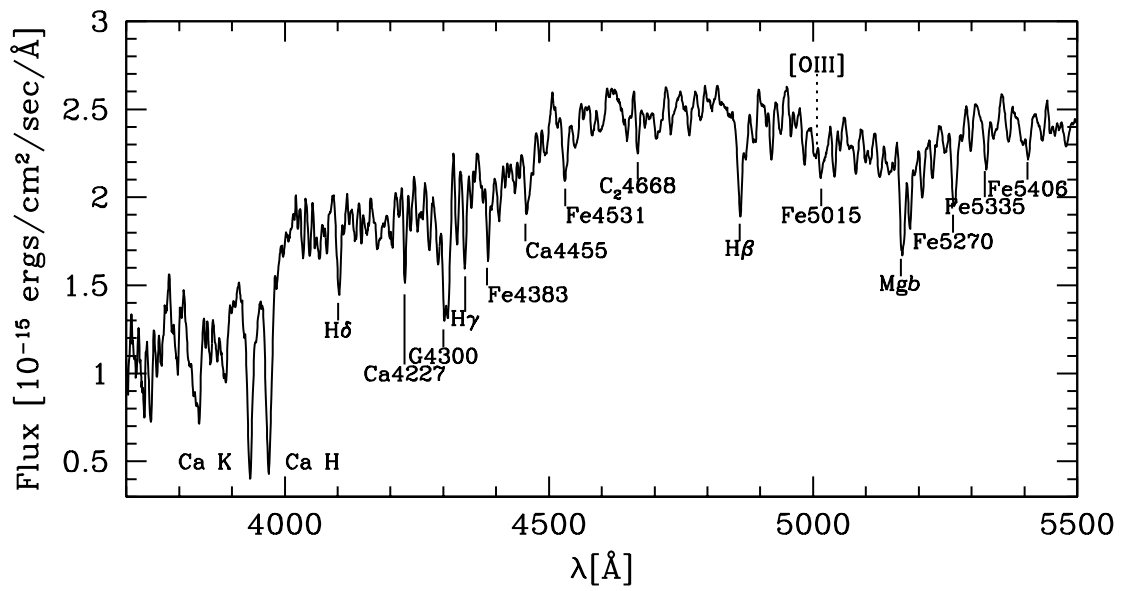


Fig. 2.— Combined spectrum using all off-axis apertures, with the center of each spectral index marked. The position of the [OIII] λ 5007 emission line (of negligible intensity in this spectrum) is also marked for reference. S/N per pixel near the $H\beta$ line is > 700 .

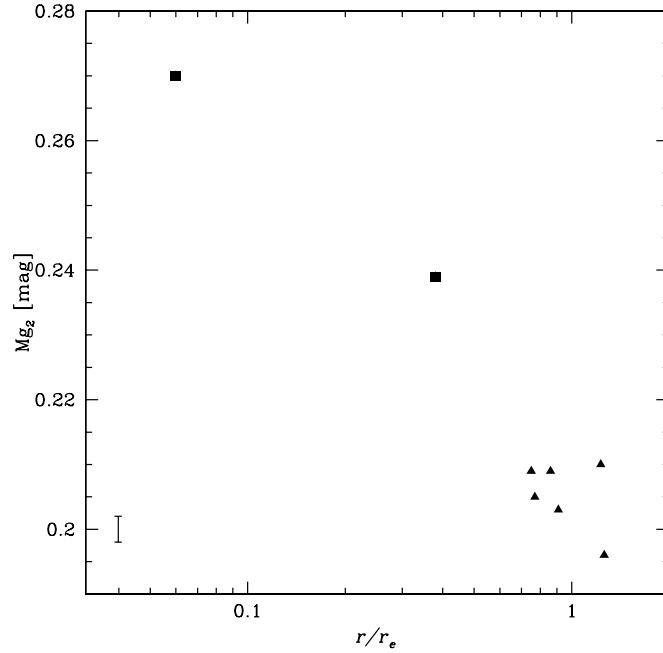


Fig. 3.— Line strength gradient of Mg_2 . Data from the on-axis spectrum is presented as squares (apertures N and P have been averaged together and appear as a single point), while data from the off-axis observations appear as triangles. Typical errors are presented in the lower left. A significant radial gradient is visible, -0.056 ± 0.004 magnitudes per decade in radius. This is in excellent agreement with the findings of Davies et al. (1993) and Kobayashi & Arimoto (1999) for Mg_2 gradients in large samples of elliptical galaxies. Within the off-axis apertures, the apertures closest to the major axis (A2–C2) have the most Mg_2 absorption.

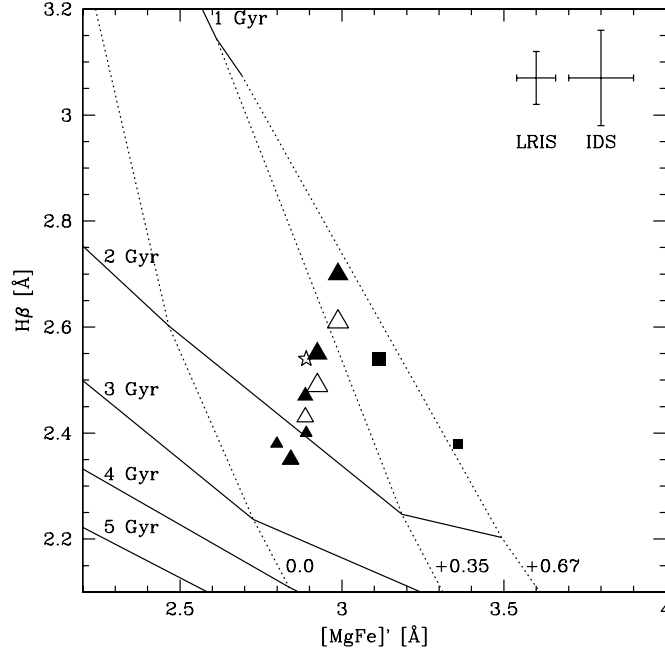


Fig. 4.— $H\beta$ vs. $[MgFe]'$. LRIS data from the off-axis (triangles) and on-axis (squares) are presented. Within each data set, point size is proportional to distance from the galaxy center. The open triangles do not include any $H\beta$ emission correction but are otherwise identical to the corresponding solid triangles. The star symbol indicates the value of these indices in the combined spectrum shown in Fig. 2. Models are from Thomas et al. (2003), with solar abundance ratios; isochrone (solid) and isometallicity (dotted) lines are labeled. Typical error bars are shown in the upper right. The LRIS error bars correspond to the total error in the text, while the IDS error bars also account for the uncertainty within the Lick/IDS system; see § 2.3 for details. Within the off-axis data set, there appears to be a radial stellar population gradient such that the outer apertures are systematically younger and more metal-rich than the apertures closest to the galactic center. The central and intermediate radius on-axis apertures are inconsistent with this picture, being more metal-rich than all but the outermost off-axis aperture, and of comparable age to the average of the off-axis apertures.

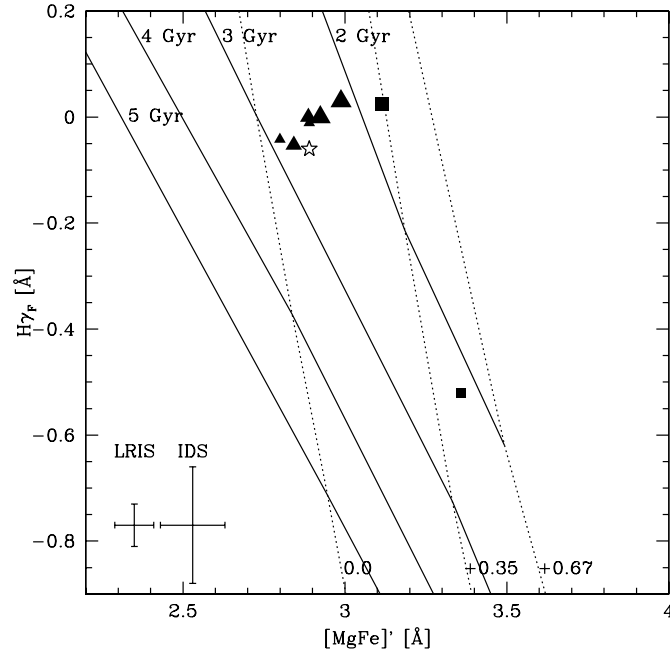


Fig. 5.— $H\gamma_F$ vs. $[MgFe]'$. Points, error bars, and models are as Fig. 3. Although qualitatively similar to the trends shown in Fig. 3, the gradient within the off-axis apertures is not statistically significant in the $H\gamma_F$ - $[MgFe]'$ plane. This figure suggests a monotonic decrease in metallicity with radius, with only slight variations in age.

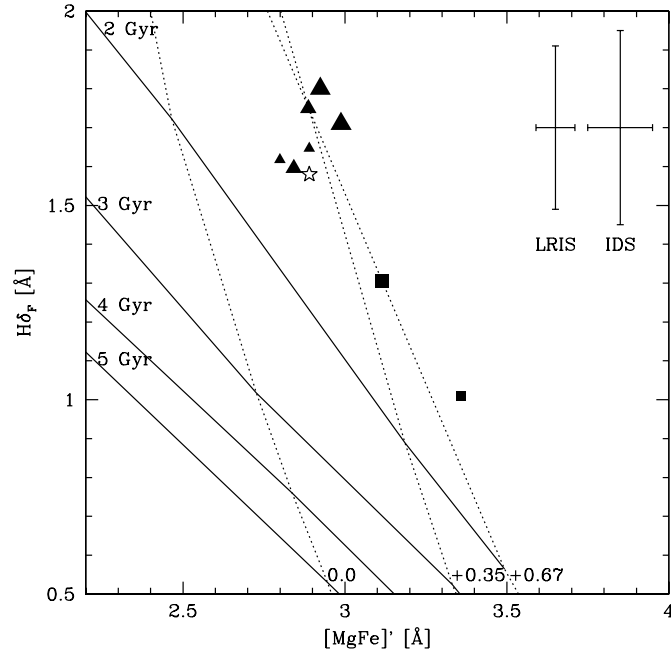


Fig. 6.— $H\delta_F$ vs. $[MgFe]'$. Points, error bars, and models are as Fig 3. Within the errors, the index measurements in the $H\delta_F$ – $[MgFe]'$ plane are consistent with metallicity decreasing with radius, with no significant age gradient.

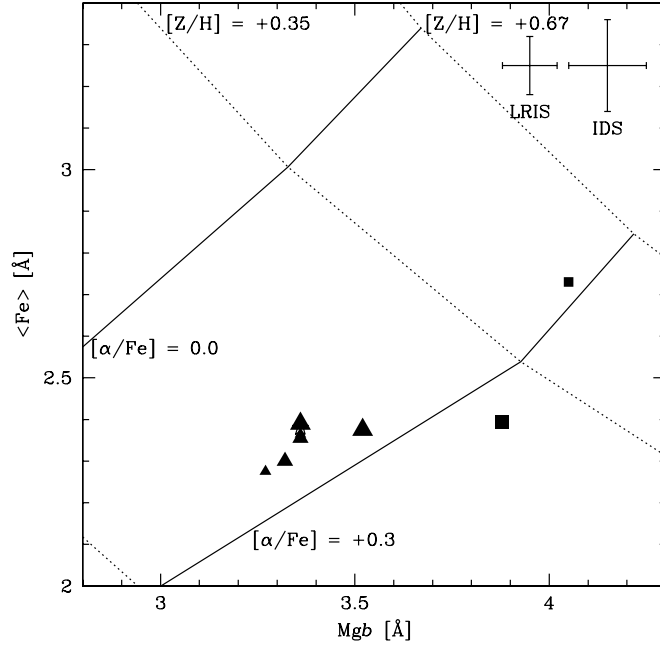


Fig. 7.— $\langle \text{Fe} \rangle$ vs. $\text{Mg } b$. Data points are as Fig 3. Also shown are 2 Gyr model grids from Thomas et al. (2003). Solid lines have constant $[\alpha/\text{Fe}]$, dotted lines have constant $[Z/\text{H}]$. Typical index errors are shown in the top right. Accounting for the differences in age, the off-axis apertures have equivalent $[\alpha/\text{Fe}]$ with the exception of aperture C2 which is enhanced by ~ 1 standard deviation with respect to the other apertures. The $r_e/8$ aperture shows an $[\alpha/\text{Fe}]$ value consistent with the off-axis apertures, while the intermediate radius apertures yield $[\alpha/\text{Fe}]$ values ~ 1 standard deviation higher than either the central or the off-axis apertures. We conclude that there is no significant radial gradient in $[\alpha/\text{Fe}]$.

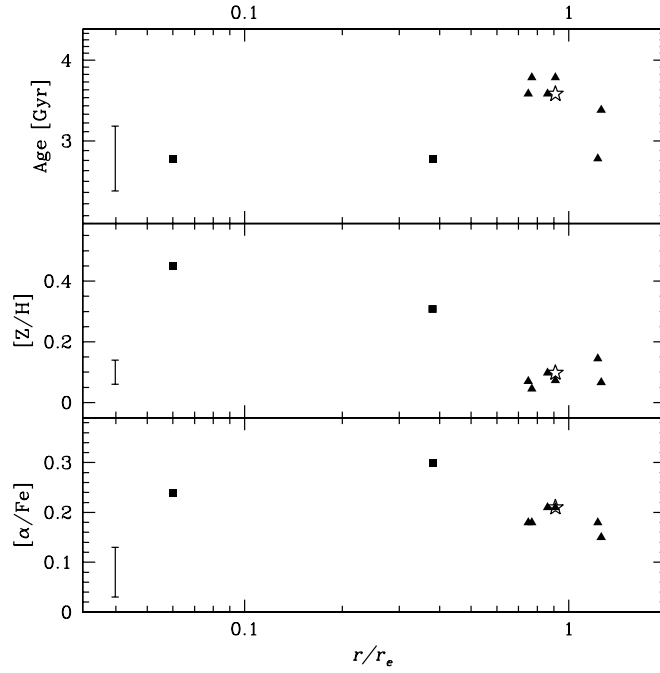


Fig. 8.— Radial gradients in age (top panel), $[Z/H]$ (middle panel), and $[\alpha/Fe]$ (bottom panel), derived from the multi-index fitting method, § 3.2. Point types are as in Fig. 3. No significant gradient is detected in age or $[\alpha/Fe]$, though the stellar populations near $0.8\text{--}0.9 r_e$ are somewhat older than the other apertures. A metallicity gradient of -0.30 ± 0.05 dex in $[Z/H]$ per decade in radius is detected, though within the off-axis apertures solely the measurements are consistent with no metallicity gradient.

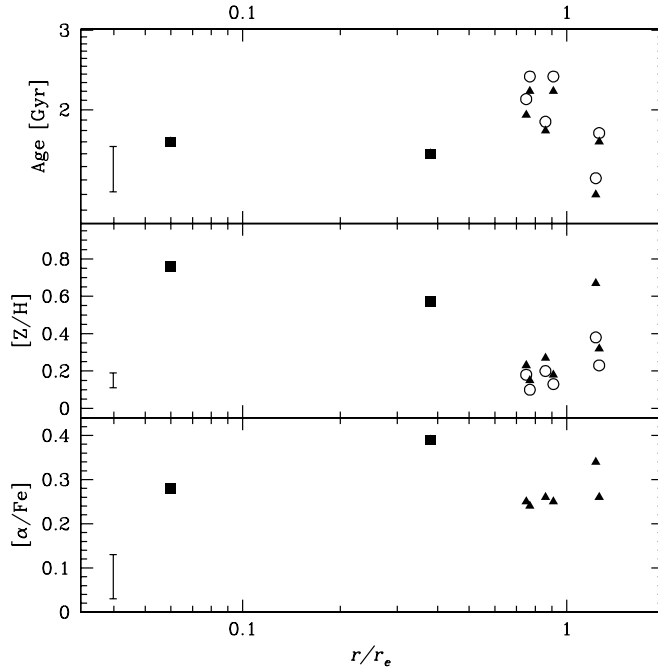


Fig. 9.— Radial gradients in age (top panel), $[Z/H]$ (middle panel), and $[\alpha/Fe]$ (bottom panel). Solid point types are as in Fig. 3, measured using the two-dimensional fitting technique of § 3.1 with $H\beta$ as the age-sensitive index. The open circle symbols represent the off-axis apertures measured by applying the multi-index fitting method to only the four indices ($H\beta$, Mgb , $Fe5270$, and $Fe5335$) used in the two-dimensional fitting technique. These fits set $[\alpha/Fe]$ to zero since the number of input indices was inadequate to fit for all three quantities. Typical error bars in each quantity are shown in the lower left of each panel. The two measurement techniques differ only by an offset of less than one standard deviation. The different results compared to Fig. 8 are entirely due to the more restricted set of indices used here. Using just these indices, the overall age gradient is unclear, though the off-axis apertures show a steep gradient becoming younger at larger radii. The overall metallicity gradient is qualitatively similar to that measured in Fig. 8, but 50% steeper in slope. In addition, the off-axis apertures show a clear gradient in the opposite direction whereas Fig. 8 showed that $[Z/H]$ remains roughly constant in these apertures. The $[\alpha/Fe]$ gradient remains negligible when measured using only this restricted set of indices.